Since January 2020 Elsevier has created a COVID-19 resource centre with free information in English and Mandarin on the novel coronavirus COVID-19. The COVID-19 resource centre is hosted on Elsevier Connect, the company's public news and information website.

Biosensors and Bioelectronics 190 (2021) 113439

Contents lists available at ScienceDirect

Biosensors and Bioelectronics

journal homepage: www.elsevier.com/locate/bios

Microfabricated potentiometric sensor for personalized methacholine challenge tests during the COVID-19 pandemic

Norhan Badr ElDin *, Mohamed K.Abd El-Rahman, Hala E. Zaazaa, Azza A. Moustafa, Said A. Hassan

Analytical Chemistry Department, Faculty of Pharmacy, Cairo University, Kasr-El Aini Street, Cairo, 11562, Egypt

ARTICLE INFO

Keywords:
Methacholine challenge test
Companion diagnostics
COVID-19
Cholinesterase activity
Potentiometric sensors

ABSTRACT

The methacholine challenge test is considered to be the gold standard bronchoprovocation test used to diagnose asthma, and this test is always performed in pulmonary function labs or doctors' offices. Methacholine (MCH) acts by inducing airway tightening/bronchoconstriction, and more importantly, MCH is hydrolyzed by cholinesterase enzyme (ChE). Recently, the American Thoracic Society raised concerns about pulmonary function testing during the COVID-19 pandemic due to recently reported correlation between cholinesterase and COVID-19 pneumonia severity/mortality, and it was shown that cholinesterase levels are reduced in the acute phase of severe COVID-19 pneumonia. This work describes the microfabrication of potentiometric sensors using copper as the substrate and chemically polymerized graphene nanocomposites as the transducing layer for tracking the kinetics of MCH enzymatic degradation in real blood samples. The in-vitro estimation of the characteristic parameters of the MCH metabolism [Michaelis–Menten constant (K_m) and reaction velocity (V_{max})] were found to be 241.041 μM and 56.8 μM/min, respectively. The proposed sensor is designed to be used as a companion diagnostic device that can (i) answer questions about patient eligibility to perform methacholine challenge tests, (ii) individualize/personalize medical dosing of methacholine, (iii) provide portable and inexpensive devices allowing automated readouts without the need for operator intervention (iv) recommend therapeutic interventions including intensive care during early stages and reflecting the disease state of COVID-19 pneumonia. We hope that this methacholine electrochemical sensor will help in assaying ChE activity in a "timely" manner and predict the severity and prognosis of COVID-19 to improve treatment outcomes and decrease mortality.

1. Introduction

In pneumonology, asthma is a common long-lasting airway disease that is associated with a high social, economic, and personal toll (Lopez et al., 2006; Omrani et al., 2016; Reddel et al., 2015). According to the World Health Organization, asthma's global prevalence is estimated to be 300 million, with a quarter million deaths reported annually (Levy et al., 2014). Ideally, asthma is suited for precision medicine due to its dynamic complexity and heterogeneity. Asthma has several components with nonlinear dynamic interactions that do not exist in all patients, which rationalizes the requirement for a precision medicine approach pointed towards enhancing the assessment and the treatment (Agusti et al., 2016; Agustí et al., 2015; Woodruff et al., 2015). Bronchoprovocation challenge testing is commonly used for assessing airflow limitations and characterizing bronchial responsiveness pathophysiology (Coates et al., 2017). Currently, the methacholine challenge test is the most common bronchoprovocation test in the clinical arena (Birnbaum and Barreiro, 2007; Cockcroft, 2007; Crapo, 2000; Popa et al., 2001). Methacholine chloride is a long-acting acetylcholine derivative that acts on muscarinic receptors on airway smooth muscle, inducing airway tightening and bronchoconstriction (National Center for Biotechnology Information, 2004).

As the goal of methacholine testing is to substantially induce bronchial constriction, the absence of preventable harm to a patient during this process is critical, so several contraindications are documented, such as chest infections and cholinesterase inhibitor drugs. The test presents a risk of cross-infection and spreading of nosocomial infections, particularly in the current era of COVID-19. Cholinesterase inhibitors either bind reversibly or non-reversibly to acetylcholinesterase and inhibit the hydrolysis of methacholine, thus increasing the availability of methacholine and aggravating its bronchoconstriction effect, which might negatively influence COVID-19 pneumonia patients.

* Corresponding author.
E-mail address: norhan.ibrahim@pharma.cu.edu.eg (N.B. ElDin).

https://doi.org/10.1016/j.bios.2021.113439
Received 15 March 2021; Received in revised form 29 May 2021; Accepted 10 June 2021
Available online 12 June 2021

The COVID-19 pandemic is considered to be the most challenging issue we have confronted since World War II, with more than 159 million cases of COVID-19 reported globally, resulting in more than 3,314,197 deaths (Worldometer, 2021). The members of the Committee of the American Thoracic Society recently raised concerns about pulmonary function testing "as a potential avenue for COVID-19 because of the potential for coughing and droplet formation" (McCormack and Kaminsky, 2020). In addition to the risk of nosocomial infection spreading, different recent studies have reported that cholinesterase level is considered as one of the prognostic factors that might be used as a useful measurement in the prediction of fatal COVID-19 (Nakajima et al., 2020, 2021; Skevaki et al., 2020; Tschoellitsch et al., 2021; Xiang et al., 2020; Zeng et al., 2021; Zhang and Guo, 2020). It was reported that cholinesterase levels were significantly lower in the severe cases than in the mild-to-moderate cases, and they were also significantly lower in the death group than in the survival group. Although the mechanism underlying cholinesterase reduction in sepsis has not yet been determined, it is thought to be affected by acute phase infections and inflammatory processes (Zivkovic et al., 2018).

Cholinesterase has been historically assayed by several techniques, such as manometric (Humiston and Wright, 1967; Kalow and Lindsay, 1955; Witter, 1962), titrimetric (Schwartz and Myers, 1958; Wilson and Cabib, 1956), photometric (Caraway, 1956; Ellman et al., 1961; Pohanka et al., 2009), fluorometric methods (Guilbault and Kramer, 1965; He et al., 2015; Li et al., 2013) and electrochemical methods (Cuartero et al., 2012, 2018; Du et al., 2011; Hart et al., 1997; Imato and Ishibashi, 1995; Mousavi et al., 2018a; Panraksa et al., 2018). The utilization of potentiometric methods presents some advantages over other techniques, including simplicity, rapidness and minor sample preparations. Advances in molecular diagnostics and molecular medicine have paved the way towards point-of-care companion diagnostic (CDx) assays (Chen et al., 2021; Gubala et al., 2012; Nayak et al., 2017; Yager et al., 2008). Parallel to these advancements in CDx, there is continuous interest in employing electrochemical methods in the development of sensors/biosensors for biomedical applications. This is driven by the *"rapid response"* and high sensitivity of electrochemical methods, the possibility of electrode miniaturization, the compatibility with current microfabrication processes, the capability of mass production, the availability of cost-effective microfabricated electrodes, the small volume sample (which is critical for dehydrated and pediatric patients) and the simplicity of use by non-specialists due to the ease of interfacing with portable readers with high cloud connectivity (Bell et al., 2019; Hassan et al., 2020; Jung et al., 2006; Moety et al., 2020; Mousavi et al., 2018b; Novell et al., 2014; Wang, 2006; Yu et al., 2018).

One of the major confrontations that should be addressed is the selection of appropriate sensor materials for potentiometric electrodes. Different ion-selective sensing membranes can be directly applied onto metal substrates (such as copper or surface treated with gold, silver, or palladium) on printed circuit boards (Anastasova et al., 2018; Moreira et al., 2016; Pei et al., 2014). Copper (Cu) substrates have been recently introduced, providing an attractive route to microscale patterns and structures needed for applications in the electronics industry and different analytical disciplines (can be patterned in a single photolithographic step such as a presensitized printed circuit), and they have a considerably lower cost than other metals. However, Cu electrodes could not be used due to the drop in the recorded electromotive force (emf) and the extensively unstable response. The loss of its optimal function is most likely due to the sensitivity of Cu to oxygen and the formation of a water layer at the interface between the ionically conducting membrane and the electronically conducting substrate, which disturbs the charge transfer process. Alternative ways for stabilizing the electrode potential and therefore extending its lifetime have been explored. One of the well-established approaches is the incorporation of an ion-to-electron transducer intermediate layer between the ion-selective membrane and the solid substrate having mixed ionic and electronic conductivity. Several nanomaterials have been synthesized to be used as ion-to-electron transducers, such as carbon nanotubes, conducting polymers, graphene and their nanocomposites (Brusic et al., 1997; Jafari et al., 2016; Özyılmaz et al., 2005; Tüken et al., 2005). Graphene (Gr), "the mother of all graphitic forms of carbon", has gained considerable attention in analytical chemistry, especially in the sensing application field, due to its chemical stability, mechanical strength and electrical conductivity. Recent progress has shown that graphene-based polymer nanocomposites display superior graphene properties. Therefore, modifying the Cu surface with graphene-based polymer nanocomposites in potentiometric measurements is expected to enhance both the stability of the substrate in the long term and improve the potential instability of solid-contact ISEs(Boeva and Lindfors, 2016; Liang et al., 2015; Yan et al., 2016).

In this work, we have developed a MCH selective potentiometric medical device based on graphene nanoparticles as a transducer and CX4 as an ionophore for continuous monitoring of MCH in real blood samples. In the first phase, the proposed sensor performance and measurement reproducibility were compared with those of a free graphene-based polymer electrode according to IUPAC recommendations. Then, the efficiency of the selected microfabricated electrode to determine MCH was tested in its pharmaceutical formulation. In the last phase, we developed a potentiometric assay for AChE activity using the considered sensor to continuously track the enzymatic hydrolysis of MCH, and a comparative analysis was conducted comprising the monitoring of acetylcholine (ACh) hydrolysis. The established approach has been used to extract comparative results by calculating different kinetic parameters, such as K_m and V_{max}. Finally, we have highlighted the development of a companion diagnostic device that could be used to evaluate the likelihood of asthma patients undergoing methacholine challenge tests. Additionally, it could be one of the useful predictors of severity and prognosis of COVID-19 pneumonia.

2. Experimental

2.1. Chemicals and electrochemical instrumentations

All the chemicals and electrochemical instrumentation details are mentioned in the Supplementary information section S-1.

2.2. Copper electrode microfabrication using photolithography

The microfabricated sensors were fabricated as described in the literature (La Belle et al., 2007). A photomask design with a specified electrode pattern was performed using Computer-Aided Design software and printed onto a transparent sheet, which was placed on a photoresist-coated wafer. UV light (360 nm) struck the photoresist for 30 s, where exposure to UV radiation removed the uncovered positive photoresist. The areas exposed to light became more soluble in the developer. These areas were dissolved in the developer (0.25 M sodium hydroxide), while the unexposed resist molecules remained on the wafer. Then, Cu wet etching was performed using a 1.0 M solution of $NH_4S_2O_8$ at 40 °C under agitation. After a photoresist was no longer needed, it was removed from the substrate using a liquid resist stripper (acetone). Then, the designed electrodes were washed with isopropanol, glacial acetic acid followed by water to remove any impurities on the surface. A diagram presenting the steps of the fabrication procedure is shown in Supplementary Information Schemes S–1.

2.3. Preparation of graphene-based polymer nanocomposites

Graphene/polyvinyl chloride (PVC) nanocomposites were synthesized by the solution-blending method as reported in the literature (Hasan and Lee, 2014); PVC (1.5 g) was completely dissolved in 50.0 mL THF with the aid of 1-(2-Nitrophenoxy)octane (2-NPOE). Graphene (0.015 g) was mixed with the above solution under continuous stirring and occasional shaking in an ultrasonic bath for the appropriate

dispersion of these nanomaterials inside the THF solution of PVC to obtain a homogeneous PVC/graphene solution.

2.4. Fabrication of solid-state ion-selective electrodes

The microfabricated Cu electrodes were modified by casting 15.0 μL of graphene/PVC nanocomposite dispersion and left for 24 h until the solvent evaporated. Then, the ion-selective sensing membrane solution was directly applied on the modified copper electrode and left to dry overnight. The master PVC ion-selective membrane (ISM) containing 32.88% PVC, 65.67% 2-NPOE, potassium; tetrakis (4-chlorophenyl) bromide (KTCPB) (5.0 mmol kg^{-1}, 0.16%) and calix [4]arene (CX4) (10 mmol kg^{-1}, 1.29%) was mixed in six mL of tetrahydrofuran (THF). Before using the sensor for the first time, the sensor is immersed in a 0.1 mM solution of MCH for 3 h at 25 °C as preconditioning step. Similarly, the ACh-selective electrode was obtained by drop-casting the previously prepared ISM onto a separate microfabricated electrode and then preconditioned in 0.1 mM ACh before its use.

To investigate the effect of the graphene/PVC nanocomposites on the potential stability, MCH-ISE was prepared without the Gr layer, Cu/ISM. Scheme 1 illustrates the structure of the Cu/ISM and Cu/Gr/ISM sensors.

2.5. Electrode measurements

The proposed ISE in conjugation with the reference electrode was immersed in a 1.0 mM MCH solution (20 mM phosphate buffer, pH 7.4). A photo presenting the whole potentiometric cell assembly is shown in Supplementary Information Schemes S–2. A calibration curve was obtained by successive dilution method through measuring the emf of the prepared standard solution (1.0 mM MCH) with a repeated removal of an aliquot of the MCH solution and addition of phosphate buffer solution. (pH = 7.4) with continuous emf measurements. The electrode performance was validated in accordance with IUPAC recommendations (Buck and Lindner, 1994).

2.6. Kinetic monitoring of substrate hydrolysis by blood cholinesterase

Aliquots of the pure AChE enzyme solutions, containing 5–25 U/mL, were added to 10 mL of 1.0 mM MCH and ACh solution in buffer solution (pH = 7.4). The enzyme activity was estimated by monitoring the change in the potential within the reaction time. Then, real sample (extracted red blood cell acetylcholinesterase, RBCs-AChE) was prepared as described in the literature by Hammond et al. (2003) with some modifications. Briefly, 4 mL of blood samples were centrifuged at 3000 rpm for 15 min to separate plasma and buffy coat from the RBCs layer. Then, RBCs were lysed using cold water, vortexed and placed at 4 °C for 10 min. Then, RBC membranes were isolated by repeating the centrifugation process (15,000 rpm, 20.0 min) for 8–10 cycles followed by washing with phosphate-buffered saline (pH 7.4) until they were just light pink and then suspended in phosphate buffer at the desired concentration.

The hydrolytic reaction kinetics were determined according to the following procedures: (i) In a thermostable vessel, the electrode potential was stabilized in buffer solution (pH = 7.4); (ii) a proper concentration of the substrate was added; and (iii) after restabilization of the potential, solubilized RBC ghosts were added, and the decline in emf values was recorded continuously. (iv) The concentration-time curve was constructed by conversion of the potential kinetic curve using the corresponding regression equation. (v) Kinetic data analysis allows the determination of different parameters, such as V_{max} and K_m. With the aim of evaluating the reliability of our analytical procedure, a side-by-side comparison for monitoring the catalytic activity of AChE was performed using ACh (natural substrate) and MCH (synthetic substrate). Monitoring ACh hydrolysis was performed using the previously described ACh-selective electrode.

3. Results and discussion

3.1. Ion-selective electrode sensing mechanism

Our proposed point-of-care companion diagnostic sensor is based on potentiometric (voltage) measurements at open-circuit potential, which consist of a reference electrode and an ion-selective electrode (microfabricated working electrode) that are submerged in the analyte bulk and are connected to a potentiometer with high input impedance. Under virtually zero current conditions, the ISE potential is measured in relation to the reference electrode of a constant independent half-cell potential. The potential generated is related to the activity of the analyte ion. The phase boundary potential is produced at the ISM interface and sample bulk by partitioning of the target ion between the two phases, resulting in separation of charge. The magnitude of this potential is

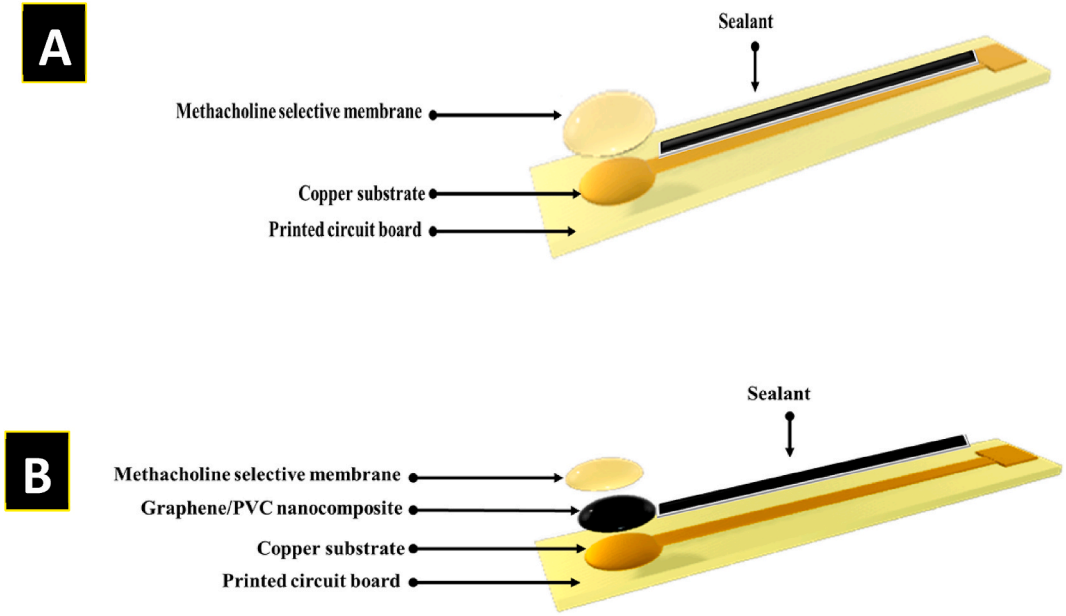

Scheme 1. A diagram for the final microfabricated (A) Cu/ISM and (B) Cu/Gr/ISM electrochemical sensor showing each layer separately.

governed by the Nernst equation: $emf = E^{\circ} + \left(\frac{RT}{zF}\right) \ln a$.where a tenfold change in activity with z charge results in a 59.2 mV/z change in the measured emf.

3.2. Optimization of the sensing ion selective membrane

The ISM responsible for the sensing mechanism consists of a plasticized polymeric membrane impregnated with a lipophilic ion exchanger and an ionophore. The reason behind the selection of each component and the preparation ratio in the ISM is explained briefly; (a) PVC was used as the polymeric matrix which provides an inert solid support in which the rest of membrane components are embedded, (b) 2-NPOE was used as a plasticizer, in particular, it is a chemically inert liquefying agent with a high dielectric constant (~24) which increases the diffusion mobility of the ion pair inside the ISM allowing homogeneous dissolution. As well reported in the literature regarding the optimum mechanical properties of the membrane and the solubility of the active sensing ingredients (Athavale et al., 2015; Bakker et al., 1999; Johnson and Bachas, 2003; Zou et al., 2014), we have used a 1:2 mass ratio of PVC and plasticizer, (c) the sensor was fabricated using KTCPB as ion exchanger, the high degree of lipophilicity of KTCPB (log P ~ 10.42) will decrease the co-extraction of the ion exchanger together with the target ion to the aqueous sample phase and consequently the detection limit and lifetime of the membrane sensor will be improved (Bakker et al., 1999; Schaller et al., 1994; Telting-Diaz and Bakker, 2001), (d) CX4 was selected as ionophore, the incorporation of CX4 into ISM increases signal stability, which is attributed to the high binding affinity between CX4 and MCH. Accordingly, the activity of MCH was buffered to a low level in the membrane, and the release of MCH into the sample bulk was dramatically reduced. To the best of our best knowledge, no CX4 for detecting MCH has been reported so far. However, it is interesting to note that CX4 has been reported to have striking complexation properties towards linear quaternary ammonium organic cations (Danil de Namor et al., 1998; Hong et al., 2007; Späth and König, 2010). In our initial experiments, we have screened three commercially available calixarenes; CX4, calix [6]arene and 4-tert-butylcalix [8]arene to identify a suitable MCH ionophore, full investigation is presented in Supplementary information section S-2 (Fig. S-1). Based on the principle of electroneutrality in the bulk of the ISM(Bakker et al., 1997; Bühlmann et al., 1998; Jansod et al., 2016; Johnson and Bachas, 2003), we have used ionophore-to-ionic site molar ratio (2:1) which proved to exhibit enhanced selectivity for the target ions. Taking all this into account, the sensor containing 32.88% PVC, 65.67% 2-NPOE, 0.16% KTCPB and 1.29% CX4 was used.

3.3. Performance characteristics of Cu-based microfabricated sensors

Our experimental work was designed such that we compared the analytical performance of the Cu/Gr/ISM with that of a blank Cu/ISM in accordance with IUPAC protocols (Buck and Lindner, 1994). The recorded emf values were plotted against logarithmic concentrations, as presented in Fig. 1A. Cu/Gr/ISM had a wider linear dynamic range (1.0×10^{-3} to 2.0×10^{-7} M versus 1.0×10^{-3} to 2.0×10^{-6} M) with a close to Nernstian response (average slope) (55.253 mV/decade versus 50.529 mV/decade) compared to the transducer-free ISE. Moreover, the detection limit was extended to 7.90×10^{-8} M for Cu/Gr/ISM, which was approximately one order of magnitude lower than that of the blank Cu/ISM. A comparison of the performance characteristics of the two sensors is shown in Table 1. The time trace of the calibration curves is presented in Fig. 1B. The response time for the Cu/Gr/ISM sensor was

Table 1
Metrological parameters (regression and validation data) of the two proposed sensors for methacholine determination.

Parameter	Cu/Gr/ISM	Cu/ISM
Slope (mV/decade) ± SD[a]	55.253 ± 0.2	50.529 ± 1.1
Intercept (mV) ± SD	352.88 ± 1.2	243.03 ± 3.1
LOD (M)[b]	7.9×10^{-8}	8.9×10^{-7}
Response time (s)	7 ± 2	20 ± 5
Concentration range (M)	1.0×10^{-3} to 2.0×10^{-7}	1.0×10^{-3} to 2.0×10^{-6}
Stability (months)	2.0 ± 0.2	1.0 ± 0.4
Correlation coefficient	0.9997	0.9993
Accuracy ± %RSD[c]	100.08 ± 0.8	99.87 ± 1.3
Repeatability[d]	0.8	1.6
Intermediate precision[d]	1.0	2.1

[a] Average of three determinations.
[b] Limit of detection (measured by interception of the extrapolated arms of nonresponsive and Nernstian segments of the calibration plot of Fig. 1.
[c] Accuracy (n = 3), average of three concentrations (5×10^{-3}, 5×10^{-4} and 5×10^{-5} M).
[d] The repeatability and intermediate precision (n = 3), RSD% of concentrations (1.0×10^{-3}, 1.0×10^{-4} and 1.0×10^{-5} M).

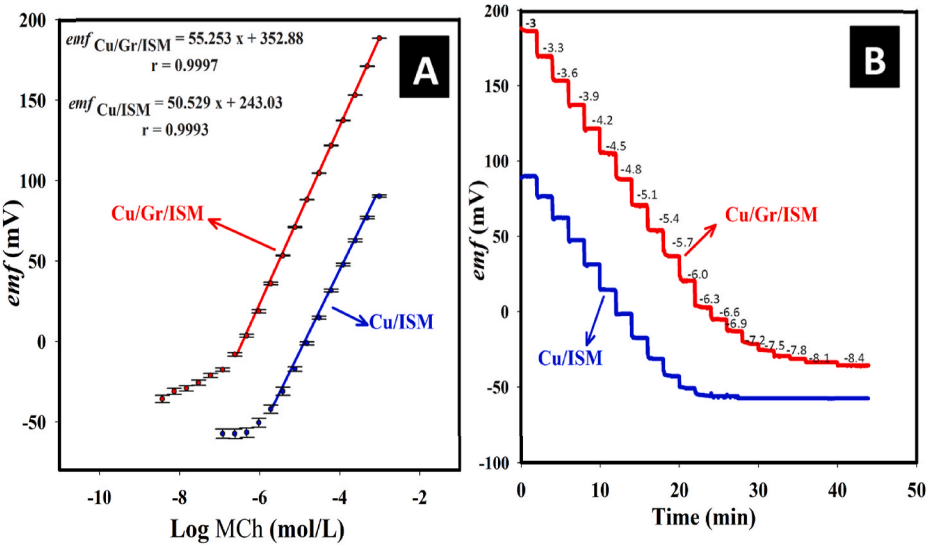

Fig. 1. (A) Profile of the measured potential in mV versus log concentrations of methacholine obtained with Cu/ISM and Cu/Gr/ISM. The emf values were recorded in phosphate buffer (pH = 7.4) at room temperature (N = 3). (B) Potential−time curves of both sensors were recorded for decreasing concentrations of methacholine; Logarithmic methacholine concentrations are indicated on the traces.

less than 7 s. On the other hand, the Cu/ISM sensor exhibited a longer time to obtain stable emf values (approximately 20 s).

Moreover, the sensor reproducibility was evaluated by carrying out calibrations by three different Gr/PVC Cu-based sensors and three different blank Cu-ISE sensors. Then, the slope and standard potential (E_0) were calculated. The average slope values of the three Cu/Gr/ISM electrodes were 56.2 ± 0.4 mV decade^{-1} with a standard potential of 353.5 ± 4.0 mV, while the corresponding values between the three Cu/ISM electrodes were 50.0 ± 3.2 mV decade^{-1} and 240.0 ± 10.2 mV. The stability of the sensor signal was evaluated, as presented in Fig. 2A. In the absence of the transducer layer, a fluctuation in the potential signal was observed, and the signal drift was high at ~11.14 ± 4.51 mV h^{-1}, which was reduced to 0.87 ± 0.05 mV h^{-1} with ISEs modified with a graphene/PVC transducer layer. One possible explanation for solid-contact ISE potential drift with time has been accredited to the development of a water layer beneath the ISM, which exerts a remarkable effect on the electrode potential. The water layer test is regarded as a significant validation stage in solid contact ISE characterization. This test was carried out by measuring the potential of 0.1 mM MCH for 1 h, then in 10.0 mM ACh (interfering ion) for 1 h, and finally back to the primary ion solution for another 1 h while emf values were recorded. As presented in Fig. 2B, obvious potential drifts were observed in the case of the Gr-free sensor. With the introduction of the Gr layer, the potential drifts were dramatically diminished. This may be attributed to the enhanced adhesion by the intermixed layer's formation between the Gr contact and the ISM due to its hydrophobicity, as has been pointed out recently that hydrophobic effects play a crucial role in the minimization of potential drift (He et al., 2017; Nayak et al., 2017; Rousseau and Bühlmann, 2021). The surface characterization of both Cu/ISM and modified Cu/Gr/ISM interfaces was performed by electrochemical impedance spectroscopy (Supplementary information section S-3, Fig. S-2). Interestingly, the results show that the Cu/Gr/ISM sensor offers favorable performance characteristics compared with Cu/ISM, such as a Nernstian slope, linear range, sensitivity and stability of response, which are important characteristics of all ion-selective electrodes. For these reasons, Cu/Gr/ISM was effectively used for analyzing MCH in its Povocholine® powder (Supplementary Information section S-4, Tables S–1) and for enzymatic activity. Additionally, the pH and temperature effects on the potentiometric measurements was carefully investigated as presented in Supplementary information section S-5 (Fig. S-3). The obtained results showed no considerable change in the calibration characteristics in the temperature range of 25 °C–40 °C and in the pH range of 3.0–9.0 which enables emf recording while monitoring the enzymatic reaction.

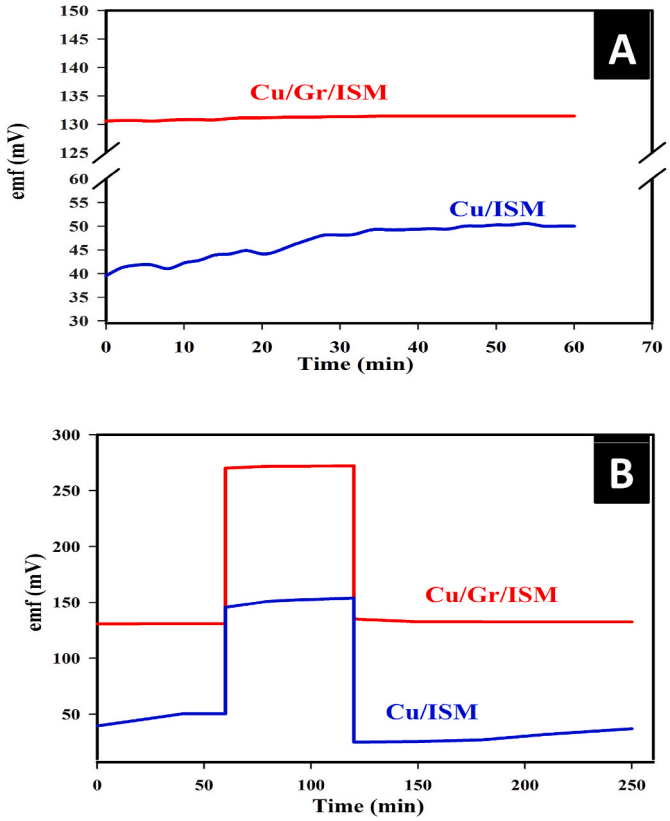

Fig. 2. (A) Short-term potential stability of Cu/ISM and Cu/Gr/ISM upon measuring in 0.1 mM methacholine solution for 1 h. In the presence of the Gr layer, the potential drift was reduced to 0.87 ± 0.05 mV h^{-1}. (B) Water layer test of Cu/ISM and Cu/Gr/ISM. Potential drift is recorded when using Cu/ISM indicating the accumulation of the water layer between the sensing membrane and the Cu substrate.

3.4. A comparison between the proposed sensor and reported methods

Since MCH is an analytically challenging compound, a few analysis methods have been reported for MCH quantification. Supplementary Information Tables S–2 represents a comparison of the proposed potentiometric method with other reported methods. The proposed sensor offers several opportunities in reference to the other reported ones in terms of linearity and LOD.

3.5. Graphene/PVC nanocomposite-based electrode selectivity study

A separate solution method was used to calculate the selectivity of the Cu/Gr/ISM toward MCH versus MCH metabolite (β-methylcholine), MCH potential impurity (choline) and interfering ions that are present in biological fluids. Fig. 3 shows the calibration curves for the selected interferents, then the selectivity coefficient values, the log $K^{pot}_{MCh,I}$, were calculated in Supplementary Information Tables S–3. The obtained values indicate high Cu/Gr/ISM(CX4) selectivity towards MCH, an explanation for the improved selectivity toward MCH and the non-significant interference of MCH metabolites is credited to the higher lipophilic character of MCH and hence the decreased partitioning of metabolites into the ISM. This discrimination over the interferents allows accurate monitoring of MCH during the initial enzymatic hydrolysis.

3.6. Potentiometric monitoring of cholinesterase-catalyzed hydrolysis of methacholine

To provide comparative information, we experimentally studied the AChE-catalyzed enzymatic hydrolysis of MCH and ACh substrates

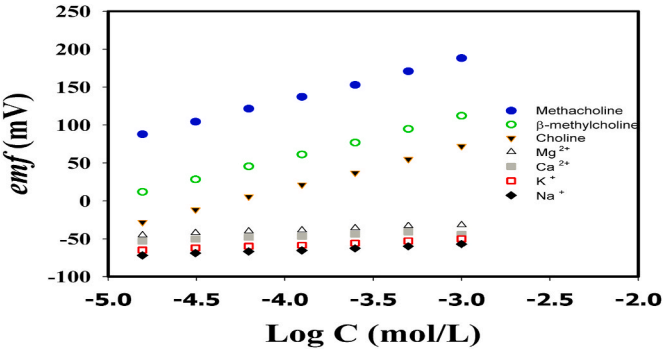

Fig. 3. Calibration plots obtained for methacholine, potentially interfering ions and some physiologically-relevant concentration of ions in blood using Cu/Gr/ISM sensor. Calibration curves were obtained by successive dilution and Nernstian response was confirmed in the concentration range where selectivity was measured.

monitored by ion-selective electrodes. The addition of AChE to each substrate-buffer solution resulted in a decrease in emf readings, indicating that the concentration of each substrate in the solution was decreasing due to enzymatic hydrolysis. Under the optimized conditions (pH = 7.4 and temperature = 25 °C), a calibration curve for AChE was carried out by plotting the measured potential change after a fixed time of enzyme addition against enzyme concentration in the range of 5.0–25.0 U/mL with a fixed concentration of substrate 1 mM. The response showed a good linearity over the activity range 5–25 U/mL for MCH and ACh, Fig. 4A. As a second step, the developed disposable sensors were applied for assaying ChEs activity in the prepared RBCs membrane ghosts. The AChE activity of the prepared solution was found to be 7.65 ± 0.3U/mL which is in a good agreement with the specification of reported ones (Burman, 1961; Dafferner et al., 2017; J. Whitfield, 2001). Then, Initial hydrolysis rates of the substrates ACh and MCH catalyzed by the RBCs-AChE were experimentally obtained at increasing substrate concentrations using a fixed amount of the enzyme. Emf measurements were converted to represent MCH concentrations utilizing the Nernst equation, and the quantified conversion concentrations decreased from 1.00 mM to 0.12 mM in a span of an hour (Fig. 4B). The kinetic profile of methacholine was recorded three times using three different Cu/Gr/ISM sensors, showing high reproducibility (Fig. 4C). This enables kinetic constant estimation (K_m and V_{max}), which is descriptive for each substrate-enzyme system. The acceptable fittings and reliable values of the kinetic constants are provided by the considerable number of experimental points describing the Michaelis–Menten plot (Fig. 4D). The fit provided values of 241.041 μM and 56.8 μM/min for MCH and 102.18 μM and 72.198 μM/min for ACh for K_m and V_{max}, respectively. As expected, the Km value for MCH as the substrate was found to be higher with respect to the values obtained for ACh (natural substrate), suggesting a higher preference for ACh to the corresponding enzyme. These results are attributed to the introduction of a methyl group on the beta position of acetylcholine relative to the quaternary ammonium group, which provides a shielding effect that inhibits nucleophilic attacks and decreases the dipole activity of the ester function and hence slows down the enzymatic hydrolysis process, leading to substantial changes in the pharmacological profiling of the drug. In contrast to ACh, MCH is hydrolyzed by acetylcholinesterase only, and its hydrolysis rate is noticeably lower than that of ACh. Consequently, the duration of MCH action is much longer than that of ACh. To prove that the decline in the emf values was due to ChE enzymatic action and not due to a drift in the sensor response, chlorpyrifos oxon (an AChE inhibitor) was spiked into RBC ghosts followed by the addition of substrate, and the potential was stable, indicating complete blocking of AChE and inhibiting its activity.

Considering the highly integrated real-time analyzers, the established sensor can be used to track the enzyme activity through the kinetic curve, eliminating the constraints introduced by the multiple sampling times, aliquots withdrawn for analysis and sample cleanup considerations. Second, the enhanced convenience, signal reproducibility, portability and cost-effectiveness of the fabricated sensor assisted the initial implementation of the CDx in hospitals; consequently, this result could significantly contribute to the revolutionization of the diagnostic kits by which apnea and COVID-19 pneumonia could be predicted.

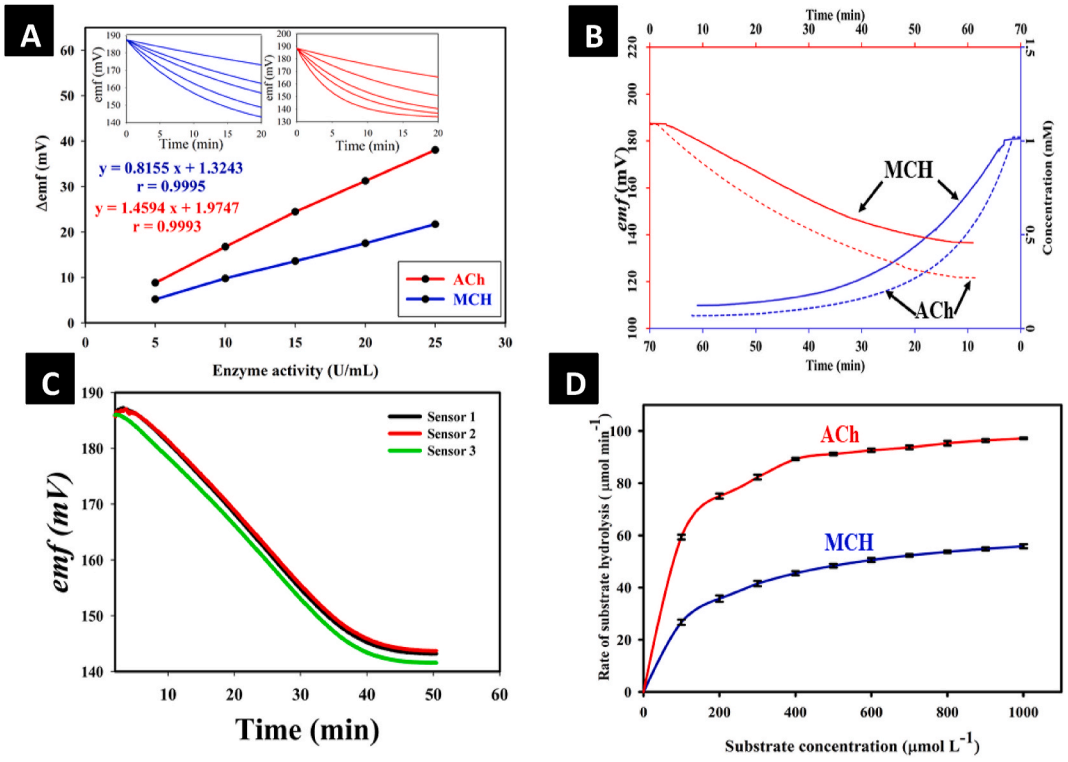

Fig. 4. (A) The linearity range of Δemf versus AChE activity using 1 mM MCH and ACh as substrates. Inset: plot of the change in the potential versus the reaction time using different AChE concentrations (5–25 U/mL). (B) Degradation of 1.0 mM methacholine and acetylcholine by blood cholinesterase monitored by Cu/graphene/ISM sensor: as the RBCs-AChE (7.65 U/mL) was spiked into substrate solution, enzymatic hydrolysis rapidly started followed by decay in the substrate concentration. The blue colored plot shows the corresponding kinetic curve obtained by transforming the potential data into concentration using the calibration graph. Response curves shifted vertically relative to one another for the sake of improved clarity. (C) Superimposed kinetics profile of methacholine using three Cu/Gr/ISM sensors that ensure the reproducibility of sensors. (D) Kinetic studies show the rate of enzymatic degradation of methacholine and acetylcholine in RBCs ghost over a range of substrate concentrations (0–1000 μM). A nonlinear fit used to determine the Michaelis–Menten V_{max} and K_m. (For interpretation of the references to color in this figure legend, the reader is referred to the Web version of this article.)

4. Conclusions

The utilization of microfabricated potentiometric sensors that are able to "sense" and "monitor" has paved the way from discrete samples and classical off-line methods to fully integrated real-time analyzers. In this contribution, we have designed a microfabricated Cu-based potentiometric sensor for the determination of MCH in pharmaceutical formulations and blood samples. The proposed sensor was developed by careful selection of ionophore doped membrane components and the addition of a PVC/graphene nanocomposite as a transducing layer. This modification added an enhanced potential stability to the emf signal (0.87 ± 0.05 mV $h^{-1)}$ compared to the transducer free sensor (drift $\sim 11.14 \pm 4.51$ mV h^{-1}). Moreover, it had a wider linear dynamic range (1.0×10^{-3} to 2.0×10^{-7} M versus 1.0×10^{-3} to 2.0×10^{-6} M) with an extended detection limit (7.9×10^{-8} M) and fast response time ($7 \pm$ 2sec). Furthermore, the results show standard deviation of E° as low as 1.2 indicating excellent reproducibility for a solid contact system compared to 3.1 standard deviation in E° of ion-to-electron transducer free ISE. The proposed sensor can be used as pre-test for asthma patients to indicate their eligibility to undergo challenge test. It is also considered as a CDx analyzer for real time monitoring of the rate of enzymatic hydrolysis of MCH in human blood. This last application can be used for diagnosing the severity of COVID-19 cases by assaying AChE in blood. A comparative study was performed comprising the use of ACh, and valuable comparative results have been acquired through kinetic parameters estimation (241.041 μM and 56.8 μM/min for MCH and 102.18 μM and 72.198 μM/min for ACh for K_m and V_{max}, respectively). Such sensor was exceptionally helpful in providing diagnostic information efficiently, timely and economically. The improved sensitivity of our potentiometric analyzer enables personalizing MCH challenge test for earlier diagnosis of asthma and could contribute to improve patient life expectancies during the COVID-19 pandemic.

Declaration of competing interest

The authors declare that they have no known competing financial interests or personal relationships that could have appeared to influence the work reported in this paper.

Appendix A. Supplementary data

Supplementary data to this article can be found online at https://doi.org/10.1016/j.bios.2021.113439.

References

Agustí, A., Antó, J.M., Auffray, C., Barbé, F., Barreiro, E., Dorca, J., Escarrabill, J., Faner, R., Furlong, L.I., Garcia-Aymerich, J., 2015. Personalized respiratory medicine: exploring the horizon, addressing the issues. Summary of a BRN-AJRCCM workshop held in Barcelona on June 12, 2014. Am. J. Respir. Crit. Care Med. 191, 391–401.

Agusti, A., Bel, E., Thomas, M., Vogelmeier, C., Brusselle, G., Holgate, S., Humbert, M., Jones, P., Gibson, P.G., Vestbo, J., Beasley, R., Pavord, I.D., 2016. Treatable traits: toward precision medicine of chronic airway diseases. Eur. Respir. J. 47, 410. https://doi.org/10.1183/13993003.01359-2015.

Anastasova, S., Kassanos, P., Yang, G.-Z., 2018. Multi-parametric rigid and flexible, low-cost, disposable sensing platforms for biomedical applications. Biosens. Bioelectron. 102, 668–675.

Athavale, R., Kokorite, I., Dinkel, C., Bakker, E., Wehrli, B., Crespo, G.A., Brand, A., 2015. In situ ammonium profiling using solid-contact ion-selective electrodes in eutrophic lakes. Anal. Chem. 87 https://doi.org/10.1021/acs.analchem.5b02424.

Bakker, E., Bühlmann, P., Pretsch, E., 1997. Carrier-based ion-selective electrodes and bulk optodes. 1. General characteristics. Chem. Rev. 97, 3083–3132.

Bakker, E., Bühlmann, P., Pretsch, E., 1999. Polymer Membrane Ion-Selective Electrodes-What Are the Limits? Electroanalysis. https://doi.org/10.1002/(sici)1521-4109(199909)11:13<915::aid-elan915>3.0.co;2-j.

Bell, J.G., Mousavi, M.P.S., El-Rahman, M.K.A., Tan, E.K.W., Homer-Vanniasinkam, S., Whitesides, G.M., 2019. Based potentiometric sensing of free bilirubin in blood serum. Biosens. Bioelectron. 126, 115–121.

Birnbaum, S., Barreiro, T.J., 2007. Methacholine challenge testing: identifying its diagnostic role, testing, coding, and reimbursement. Chest 131, 1932–1935.

Boeva, Z.A., Lindfors, T., 2016. Few-layer graphene and polyaniline composite as ion-to-electron transducer in silicone rubber solid-contact ion-selective electrodes. Sensor. Actuator. B Chem. 224, 624–631.

Brusic, V., Angelopoulos, M., Graham, T., 1997. Use of polyaniline and its derivatives in corrosion protection of copper and silver. J. Electrochem. Soc. 144, 436–442.

Buck, R.P., Lindner, E., 1994. Recommendations for nomenclature of ionselective electrodes (IUPAC) Recommendations 1994). Pure Appl. Chem. 66, 2527–2536.

Bühlmann, P., Pretsch, E., Bakker, E., 1998. Carrier-based ion-selective electrodes and bulk optodes. 2. Ionophores for potentiometric and optical sensors. Chem. Rev. 98, 1593–1688. https://doi.org/10.1021/cr970113+.

Burman, D., 1961. Red cell cholinesterase in infancy and childhood. Arch. Dis. Child. 36 https://doi.org/10.1136/adc.36.188.362.

Caraway, W.T., 1956. Photometric determination of serum cholinesterase activity. Am. J. Clin. Pathol. 26, 945–955.

Chen, Y., Chen, X., Li, M., Fan, P., Wang, B., Zhao, S., Yu, W., Zhang, S., Tang, Y., Gao, T., 2021. A new analytical platform for potential point-of-care testing of circulating tumor cells. Biosens. Bioelectron. 171, 112718. https://doi.org/10.1016/j.bios.2020.112718.

Coates, A.L., Wanger, J., Cockcroft, D.W., Culver, B.H., Carlsen, K.-H., Diamant, Z., Gauvreau, G., Hall, G.L., Hallstrand, T.S., Horvath, I., 2017. ERS technical standard on bronchial challenge testing: general considerations and performance of methacholine challenge tests. Eur. Respir. J. 49.

Cockcroft, D.W., 2007. Methacholine challenge. Clin. Pulm. Med. 14, 1–6.

Crapo, R.O., 2000. Guidelines for methacholine and exercise challenge testing-1999. This official statement of the American Thoracic Society was adopted by the ATS Board of Directors, July 1999. Am. J. Respir. Crit. Care Med. 161, 309–329.

Cuartero, M., Ortuño, J.A., García, M.S., García-Cánovas, F., 2012. Assay of acetylcholinesterase activity by potentiometric monitoring of acetylcholine. Anal. Biochem. 421 https://doi.org/10.1016/j.ab.2011.10.008.

Cuartero, M., Pérez, S., García, M.S., García-Cánovas, F., Ortuño, J.A., 2018. Comparative Enzymatic Studies Using Ion-Selective Electrodes. The Case of Cholinesterases. Talanta 180. https://doi.org/10.1016/j.talanta.2017.12.029.

Dafferner, A.J., Schopfer, L.M., Xiao, G., Cashman, J.R., Yerramalla, U., Johnson, R.C., Blake, T.A., Lockridge, O., 2017. Immunopurification of acetylcholinesterase from red blood cells for detection of nerve agent exposure. Chem. Res. Toxicol. 30 https://doi.org/10.1021/acs.chemrestox.7b00209.

Danil de Namor, A.F., Cleverley, R.M., Zapata-Ormachea, M.L., 1998. Thermodynamics of calixarene chemistry. Chem. Rev. 98, 2495–2526.

Du, D., Tao, Y., Zhang, W., Liu, D., Li, H., 2011. Oxidative desorption of thiocholine assembled on core-shell Fe3O4/AuNPs magnetic nanocomposites for highly sensitive determination of acetylcholinesterase activity: an exposure biomarker of organophosphates. Biosens. Bioelectron. 26 https://doi.org/10.1016/j.bios.2011.03.037.

Ellman, G.L., Courtney, K.D., Andres, V., Featherstone, R.M., 1961. A new and rapid colorimetric determination of acetylcholinesterase activity. Biochem. Pharmacol. 7 https://doi.org/10.1016/0006-2952(61)90145-9.

Gubala, V., Harris, L.F., Ricco, A.J., Tan, M.X., Williams, D.E., 2012. Point of care diagnostics: status and future. Anal. Chem. 84, 487–515.

Guilbault, G.G., Kramer, D.N., 1965. Resorufin butyrate and indoxyl acetate as fluorogenic substrates for cholinesterase. Anal. Chem. 37, 120–123.

Hammond, P.I., Kern, C., Hong, F., Kollmeyer, T.M., Pang, Y.P., Brimijoin, S., 2003. Cholinesterase reactivation in vivo with a novel bis-oxime optimized by computer-aided design. J. Pharmacol. Exp. Therapeut. 307, 190–196.

Hart, A.L., Collier, W.A., Janssen, D., 1997. The response of screen-printed enzyme electrodes containing cholinesterases to organo-phosphates in solution and from commercial formulations. Biosens. Bioelectron. 12 https://doi.org/10.1016/S0956-5663(97)00021-3.

Hasan, M., Lee, M., 2014. Enhancement of the thermo-mechanical properties and efficacy of mixing technique in the preparation of graphene/PVC nanocomposites compared to carbon nanotubes/PVC. Prog. Nat. Sci. Mater. Int. 24, 579–587. https://doi.org/10.1016/j.pnsc.2014.10.004.

Hassan, S.A., ElDin, N.B., Zaazaa, H.E., Moustafa, A.A., Mahmoud, A.M., 2020. Point-of-care diagnostics for drugs of abuse in biological fluids: application of a microfabricated disposable copper potentiometric sensor. Microchim. Acta 187, 491. https://doi.org/10.1007/s00604-020-04445-x.

He, T., Qi, L., Zhang, J., Huang, Y.L., Zhang, Z.Q., 2015. Enhanced graphene quantum dot fluorescence nanosensor for highly sensitive acetylcholinesterase assay and inhibitor screening. Sensor. Actuator. B Chem. 215 https://doi.org/10.1016/j.snb.2015.03.043.

He, N., Papp, S., Lindfors, T., Höfler, L., Latonen, R.-M., Gyurcsányi, R.E., 2017. Pre-polarized hydrophobic conducting polymer solid-contact ion-selective electrodes with improved potential reproducibility. Anal. Chem. 89, 2598–2605. https://doi.org/10.1021/acs.analchem.6b04885.

Hong, J., Song, J., Ham, S., 2007. Molecular recognition of ammonium ion by tetrahomodioxacalix [4] biscrown. Tetrahedron Lett. 48, 1327–1330.

Humiston, C.G., Wright, G.J., 1967. An automated method for the determination of cholinesterase activity. Toxicol. Appl. Pharmacol. 10, 467–480.

Imato, T., Ishibashi, N., 1995. Potentiometric butyrylcholine sensor for organophosphate pesticides. Biosens. Bioelectron. 10 https://doi.org/10.1016/0956-5663(95)96890-B.

Jafari, Y., Ghoreishi, S.M., Shabani-Nooshabadi, M., 2016. Polyaniline/Graphene nanocomposite coatings on copper: electropolymerization, characterization, and evaluation of corrosion protection performance. Synth. Met. 217, 220–230. https://doi.org/10.1016/j.synthmet.2016.04.001.

Jansod, S., Afshar, M.G., Crespo, G.A., Bakker, E., 2016. Phenytoin speciation with potentiometric and chronopotentiometric ion-selective membrane electrodes. Biosens. Bioelectron. 79, 114–120. https://doi.org/10.1016/j.bios.2015.12.011.
Johnson, R.D., Bachas, L.G., 2003. Ionophore-based ion-selective potentiometric and optical sensors. Anal. Bioanal. Chem. 376 (3), 328–341. https://doi.org/10.1007/s00216-003-1931-0.
Jung, S., Ji, T., Varadan, V.K., 2006. Point-of-care temperature and respiration monitoring sensors for smart fabric applications. Smart Mater. Struct. 15, 1872.
Kalow, W., Lindsay, H.A., 1955. A comparison of optical and manometric methods for the assay of human serum cholinesterase. Can. J. Biochem. Physiol. 33, 568–574.
La Belle, J.T., Gerlach, J.Q., Svarovsky, S., Joshi, L., 2007. Label-free impedimetric detection of glycan– lectin interactions. Anal. Chem. 79, 6959–6964.
Levy, M., Andrews, R., Buckingham, R., Evans, H., Francis, C., Houston, R., Lowe, D., Nasser, S., Paton, J., Puri, N., 2014. Why Asthma Still Kills: the National Review of Asthma Deaths (NRAD).
Li, Wenhua, Li, Wang, Hu, Y., Xia, Y., Shen, Q., Nie, Z., Huang, Y., Yao, S., 2013. A fluorometric assay for acetylcholinesterase activity and inhibitor detection based on DNA-templated copper/silver nanoclusters. Biosens. Bioelectron. 47 https://doi.org/10.1016/j.bios.2013.03.038.
Liang, R., Yin, T., Qin, W., 2015. A simple approach for fabricating solid-contact ion-selective electrodes using nanomaterials as transducers. Anal. Chim. Acta 853, 291–296.
Lopez, A.D., Shibuya, K., Rao, C., Mathers, C.D., Hansell, A.L., Held, L.S., Schmid, V., Buist, S., 2006. Chronic obstructive pulmonary disease: current burden and future projections. Eur. Respir. J. 27, 397. https://doi.org/10.1183/09031936.06.00025805.
McCormack, M.C., Kaminsky, D.A., 2020. Pulmonary Function Laboratories: Advice Regarding COVID-19. ATS Dis. Relat. Resour [WWW Document]. https://www.thoracic.org/professionals/clinical-resources/disease-related-resources/pulmonary-function-laboratories.php. accessed 2.3.21.
Moety, E.A., Abou Al-Alamein, A., Fawaz, E., Abdelrahman, M.K., 2020. A companion diagnostic for personalizing mivacurium at the point-of-care. J. Electrochem. Soc. 167 (8) https://doi.org/10.1149/1945-7111/ab927e.
Moreira, F.T.C., Ferreira, M.J.M.S., Puga, J.R.T., Sales, M.G.F., 2016. Screen-printed electrode produced by printed-circuit board technology. Application to cancer biomarker detection by means of plastic antibody as sensing material. Sensor. Actuator. B Chem. 223, 927–935.
Mousavi, M.P.S., Abd El-Rahman, M.K., Mahmoud, A.M., Abdelsalam, R.M., Bühlmann, P., 2018a. In situ sensing of the neurotransmitter acetylcholine in a dynamic range of 1 nM to 1 mM. ACS Sens. 3, 2581–2589.
Mousavi, M.P.S., Ainla, A., Tan, E.K.W., El-Rahman, M.K.A., Yoshida, Y., Yuan, L., Sigurslid, H.H., Arkan, N., Yip, M.C., Abrahamsson, C.K., 2018b. Ion sensing with thread-based potentiometric electrodes. Lab Chip 18, 2279–2290.
Nakajima, K., Abe, T., Saji, R., Ogawa, F., Taniguchi, H., Yamaguchi, K., Sakai, K., Nakagawa, T., Matsumura, R., Oi, Y., Nishii, M, Takeuchi, I, 2021. Serum cholinesterase associated with COVID-19 pneumonia severity and mortality. J Infect 82 (2), 282–327. https://doi.org/10.1016/j.jinf.2020.08.021.
Nakajima, K., Abe, T., Saji, R., Ogawa, F., Taniguchi, H., Yamaguchi, K., Sakai, K., Nakagawa, T., Matsumura, R., Oi, Y., Nishii, M, Takeuchi, I, 2021. Serum cholinesterase associated with COVID-19 pneumonia severity and mortality. J. Infect. 82 (2), 282–327. https://doi.org/10.1016/j.jinf.2020.08.021.
National Center for Biotechnology Information, 2004. PubChem Compound Summary for CID 1993. Methacholine [WWW Document]. PubChem Database. URL. https://pubchem.ncbi.nlm.nih.gov/compound/Methacholine. accessed 3.2.21.
Nayak, S., Blumenfeld, N.R., Laksanasopin, T., Sia, S.K., 2017. Point-of-Care diagnostics: recent developments in a connected age. Anal. Chem. 89, 102–123. https://doi.org/10.1021/acs.analchem.6b04630.
Novell, M., Guinovart, T., Blondeau, P., Rius, F.X., Andrade, F.J., 2014. A paper-based potentiometric cell for decentralized monitoring of Li levels in whole blood. Lab Chip 14, 1308–1314.
Omrani, A., Rostami, H., Minaee, R., 2016. Electrochemical synthesis of polypyrrole/polyhedral oligomeric silsesquioxane nanocomposite on copper for corrosion protection. Prog. Org. Coating 90, 331–338. https://doi.org/10.1016/j.porgcoat.2015.11.001.
Özyılmaz, A.T., Tüken, T., Yazıcı, B., Erbil, M., 2005. The electrochemical synthesis and corrosion performance of polyaniline on copper. Prog. Org. Coating 52, 92–97. https://doi.org/10.1016/j.porgcoat.2004.09.003.
Panraksa, Y., Siangproh, W., Khampieng, T., Chailapakul, O., Apilux, A., 2018. Paper-based amperometric sensor for determination of acetylcholinesterase using screen-printed graphene electrode. Talanta 178. https://doi.org/10.1016/j.talanta.2017.08.096.
Pei, X., Kang, W., Yue, W., Bange, A., Heineman, W.R., Papautsky, I., 2014. Disposable copper-based electrochemical sensor for anodic stripping voltammetry. Anal. Chem. 86, 4893–4900.
Pohanka, M., Musilek, K., Kuca, K., 2009. Progress of biosensors based on cholinesterase inhibition. Curr. Med. Chem. 16, 1790–1798.
Popa, V., Enright, P., Crapo, R., 2001. ATS guidelines for methacholine and exercise challenge testing. Am. J. Respir. Crit. Care Med. 163, 292–293.
Reddel, H.K., Bateman, E.D., Becker, A., Boulet, L.-P., Cruz, A.A., Drazen, J.M., Haahtela, T., Hurd, S.S., Inoue, H., de Jongste, J.C., Lemanske, R.F., Levy, M.L., Byrne, P.M., Paggiaro, P., Pedersen, S.E., Pizzichini, E., Soto-Quiroz, M., Szefler, S.J., Wong, G.W.K., FitzGerald, J.M., 2015. A summary of the new GINA strategy: a roadmap to asthma control. Eur. Respir. J. 46, 622. https://doi.org/10.1183/13993003.00853-2015.
Rousseau, C.R., Bühlmann, P., 2021. Calibration-free potentiometric sensing with solid-contact ion-selective electrodes. TrAC Trends Anal. Chem. (Reference Ed.) 140. https://doi.org/10.1016/j.trac.2021.116277.
Schaller, U., Bakker, E., Spichiger, U.E., Pretsch, E., 1994. Ionic additives for ion-selective electrodes based on electrically charged carriers. Anal. Chem. 66 https://doi.org/10.1021/ac00075a013.
Schwartz, M., Myers, T.C., 1958. Simple microtitrimetric constant-pH method for accurate enzyme assays. Anal. Chem. 30, 1150–1151.
Skevaki, C., Fragkou, P.C., Cheng, C., Xie, M., Renz, H., 2020. Laboratory characteristics of patients infected with the novel SARS-CoV-2 virus. J. Infect. 81, 205–212. https://doi.org/10.1016/j.jinf.2020.06.039.
Späth, A., König, B., 2010. Molecular recognition of organic ammonium ions in solution using synthetic receptors. Beilstein J. Org. Chem. 6, 32.
Telting-Diaz, M., Bakker, E., 2001. Effect of lipophilic ion-exchanger leaching on the detection limit of carrier-based ion-selective electrodes. Anal. Chem. 73 https://doi.org/10.1021/ac010526h.
Tschoellitsch, T., Dünser, M., Böck, C., Schwarzbauer, K., Meier, J., 2021. Machine learning prediction of SARS-CoV-2 polymerase chain reaction results with routine blood tests. Lab. Med. 52, 146–149. https://doi.org/10.1093/labmed/lmaa111.
Tüken, T., Yazıcı, B., Erbil, M., 2005. Polypyrrole/polythiophene coating for copper protection. Prog. Org. Coating 53, 38–45. https://doi.org/10.1016/j.porgcoat.2004.11.008.
Wang, J., 2006. Electrochemical biosensors: towards point-of-care cancer diagnostics. Biosens. Bioelectron. 21, 1887–1892.
Whitfield, J., 2001. Cholinesterase – Red Blood Cell [WWW Document]. URL. https://www.slhd.nsw.gov.au/SSWPS/fact sheets/Sheet 31.pdf. accessed 5.9.21.
Wilson, I.B., Cabib, E., 1956. Acetylcholinesterase: enthalpies and entropies of activation 1. J. Am. Chem. Soc. 78, 202–207.
Witter, R.F., 1962. A critical study of the manometric assay of cholinesterase in rat blood. Toxicol. Appl. Pharmacol. 4, 313–323.
Woodruff, P.G., Agusti, A., Roche, N., Singh, D., Martinez, F.J., 2015. Current concepts in targeting chronic obstructive pulmonary disease pharmacotherapy: making progress towards personalised management. Lancet 385, 1789–1798.
Worldometer, 2021. COVID-19 Coronavirus Pandemic; Coronavirus Cases. Worldometers. WWW Document. www.worldometers.info/coronavirus/. accessed 5.9.21.
Xiang, J., Wen, J., Yuan, X., Xiong, S., Zhou, X., Liu, C., Min, X., 2020. Potential Biochemical Markers to Identify Severe Cases Among COVID-19 Patients. MedRxiv.
Yager, P., Domingo, G.J., Gerdes, J., 2008. Point-of-care diagnostics for global health. Annu. Rev. Biomed. Eng. 10.
Yan, R., Qiu, S., Tong, L., Qian, Y., 2016. Review of progresses on clinical applications of ion selective electrodes for electrolytic ion tests: from conventional ISEs to graphene-based ISEs. Chem. Speciat. Bioavailab. 28, 72–77.
Yu, Z., Tang, Y., Cai, G., Ren, R., Tang, D., 2018. Paper electrode-based flexible pressure sensor for point-of-care immunoassay with digital multimeter. Anal. Chem. 91, 1222–1226.
Zeng, H.-L., Lu, Q.-B., Yang, Q., Wang, X., Yue, D.-Y., Zhang, L.-K., Li, H., Liu, W., Li, H.-J., 2021. Longitudinal profile of laboratory parameters and their application in the prediction for fatal outcome among patients infected with SARS-CoV-2: a retrospective cohort study. Clin. Infect. Dis. 72, 626–633. https://doi.org/10.1093/cid/ciaa574.
Zhang, L., Guo, H., 2020. Biomarkers of COVID-19 and technologies to combat SARS-CoV-2. Adv. Biomark. Sci. Technol. 2, 1–23. https://doi.org/10.1016/j.abst.2020.08.001.
Zivkovic, A.R., Decker, S.O., Zirnstein, A.C., Sigl, A., Schmidt, K., Weigand, M.A., Hofer, S., Brenner, T., 2018. A sustained reduction in serum cholinesterase enzyme activity predicts patient outcome following sepsis. Mediat. Inflamm. 2018, 1942193 https://doi.org/10.1155/2018/1942193.
Zou, X.U., Zhen, X.V., Cheong, J.H., Bühlmann, P., 2014. Calibration-free ionophore-based ion-selective electrodes with a Co(II)/Co(III) redox couple-based solid contact. Anal. Chem. 86 https://doi.org/10.1021/ac501625z.